CHEMISTRY OF MATERIALS

pubs.acs.org/cm

Article

Thiadiazole Disulfide Cross-Linked Poly(3,4-ethylenedioxythiophene) Nanoparticles: A Dual Redox Approach for Organic Cathode Batteries

Hongyi Zhang, Garrett L. Grocke, George Rose, Stuart J. Rowan,* and Shrayesh N. Patel*

Cite This: *Chem. Mater.* 2024, 36, 9959−9969

Read Online

ACCESS | Metrics & More | Article Recommendations | Supporting Information

ABSTRACT: This study focuses on the synthesis and electrochemical characterization of nanoscale particles of semiconducting poly-3,4-ethylenedioxythiophene (PEDOT) functionalized with a disulfide/thiolate redox couple, specifically 2,5-dimercapto-1,3,4-thiadiazole (DMcT), allowing for dual redox particles designed for use as an organic cathode electrode. The nanoscale PEDOT-DMcT-Li dual redox particles have specific discharge capacities in a lithium half-cell of 91.9 mAh/g (85% of the maximum theoretical specific capacity, assuming both disulfide and polaron access on PEDOT) at low C-rates. This accessible capacity is attributed to the nanoscale particle size and the integration of a semiconducting conjugated backbone, which reduces internal resistance during oxidation. Comprehensive analyses, including cyclic voltammetry and galvanostatic cycling, reveal the contribution of the two individual redox components, namely, disulfide/thiolate and PEDOT, in this redox active material. Long-term cycling stability tests further suggest minimal degradation over 400 cycles with the observed capacity decay primarily attributed to charge trapping. Using an asymmetric charge/discharge rate cycling method to mitigate charge trapping results in an increase in Coulombic efficiency as well as capacity. Moreover, asymmetric cycling improved discharge capacity retention to 69% compared with 52% under symmetric rate cycling conditions after 400 cycles, without additional chemical modifications. These findings outline the redox behavior of the PEDOT-DMcT-Li system with dual-redox properties and point to their potential use as a cathode in organic batteries.

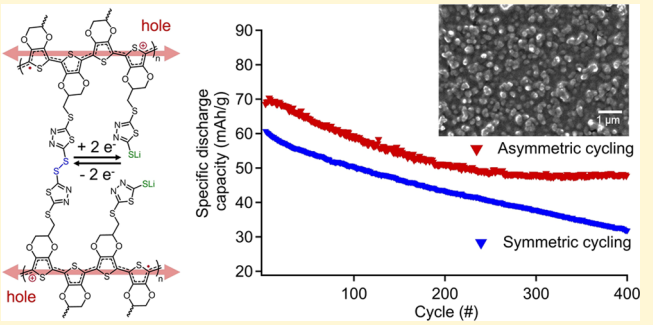

INTRODUCTION

The rise of electric mobility has imposed significant demands on lithium-ion batteries, leading to a considerable depletion of transition metal resources.[1] Reliance on transition metals has raised considerable apprehension with respect to their finite availability and the environmental impact associated with their extraction and usage.[2] Considering these concerns, organic rechargeable batteries, devoid of transition metals, emerge as eco-friendly and cost-effective alternatives with the potential to address resource scarcity and environmental sustainability issues and present a promising alternative to conventional lithium-ion batteries in the area of flexible electronics, electric vehicles, and the power grid.[3] Organic compounds that contain persistent (stable) radicals,[4] carbonyls,[5] thioether,[6,7] and organodisulfides[8,9] have emerged as a promising alternative cathode materials on account of their accessibility, sustainability, substantial theoretical capacity, and robust power characteristics.[10−14] In addition, the versatility of the molecular design and synthesis of organic active materials are well-suited for storing ions with tunable reaction kinetics and performance.[15] The versatility of these organic materials to function with multiple metal counterions enhances their potential as promising electrodes for various metal-ion batteries, including those based on lithium, sodium, and other multivalent metals.[16]

Among those redox-active organic compounds suitable for use as cathodes, a noteworthy group of materials are organosulfur compounds (OSCs). The disulfide motif (C−S−S−C), which contains a labile bond between two sulfur atoms, has a distinctive n-type redox mechanism; the S−S bond is broken after accepting two electrons, with each R−S$^-$ compensated by a countercation at a relatively low redox potential (approximately 2.2 V vs Li$^+$/Li).[17−19] Because of this multielectron redox motif, these compounds can display high specific capacities and have thus been intensively studied. Some of the first studied OSCs included tetraethylthiuram disulfide,[20] phenyl disulfide,[19] and 1,3,4-thiadiazole disulfide (TDDS) and its analogues.[9,21−23] From this early work, the TDDS derivatives, such as 2,5-dimercapto-1,3,4-thiadiazole

Received: August 25, 2024
Revised: September 16, 2024
Accepted: September 17, 2024
Published: September 30, 2024

(DMcT), stand out in their promise as redox-active small molecules. Over the years, reported studies have highlighted DMcT as a compelling candidate for cathodes in lithium batteries on account of its ability to transition between Li−S and disulfide states, offering high energy density and exceptional cyclability.[9,24−26] However, the disulfide redox reactions inherently suffer limited reversibility due to the dissolution of the produced thiolate from disulfide reduction, consequently diminishing capacity.[27] Recently, the integration of disulfide moieties into polymers or polymer networks has become a strategy to address this issue. Pioneering efforts in this domain have included the use of various redox polymers, like poly(2,4-dithiopyrimidine)[28] and poly(trithiocyanuric acid),[29] which have successfully mitigated the problem of electrode dissolution by integrating disulfide into the polymer backbone or side chains. Another benefit of immobilizing these redox-active moieties within polymer networks is the known sluggish electrochemical reaction kinetics of disulfides, characterized by rate constants of approximately 1×10^{-7} cm/s.[30,31] Immobilizing these compounds onto a substrate has been demonstrated to enhance the reversibility of the redox couple by preventing the diffusion of reduced species away from the electrode and other charged moieties necessary for recombination.

Despite this, polymer functionalization does not address the interaction between disulfides and the electrode itself. Efforts have been made to improve the performance in this aspect through electrocatalysis, utilizing additional molecular species that can accelerate charge transfer kinetics without being consumed. One notable example is the use of conjugated polymers, such as the well-studied poly(3,4-ethylenedioxythiophene), or PEDOT, to enhance both the rate of charge transfer and the reversibility of the DMcT redox couple.[30,31] Pioneering work by Oyama et al. involved electrochemically polymerizing PEDOT on a glassy carbon electrode and comparing the electrochemical activity of DMcT on coated versus bare electrodes.[22] Subsequent computational studies provided insights into the favorable thermodynamics of the system, whereby electron transfer occurs from the highest occupied molecular orbital (HOMO) of neutral PEDOT to the lowest unoccupied molecular orbital (LUMO) of oxidized forms of DMcT, facilitating DMcT reduction alongside PEDOT oxidation to a doped state.[31] Kinetic studies demonstrated a 12,000-fold increase in the redox reaction rate when using a PEDOT coated-electrode compared to a glassy carbon electrode.[26] Initial investigations showcased enhanced reactivity of DMcT solutions on a PEDOT-coated electrode and subsequent studies focused on a composite material by integrating solid DMcT into PEDOT prior to cell assembly.[30] While this electrocatalytic approach improved the overall performance, the diffusion of DMcT limited the cycling lifetime of the material.

Contrasting with the composite materials mentioned previously, one approach is to covalently functionalize conjugated polymers with redox-active components to form dual redox polymers, which combines the benefit of immobilizing the redox active component on the polymer backbone to prevent dissolution and the use of the conjugated polymer to improve reaction kinetics. Such dual redox polymers have been effectively demonstrated with various redox-active moieties. Examples include attaching terephthalate units to polythiophene,[32] creating cross-hybrids of quinone and polyaniline,[33] and combining PEDOT with quinone[34] or stable nitroxide radical compounds (TEMPO).[35] More recently, the covalent attachment of DMcT to electropolymerized poly(2,3-dihydrothieno[3,4-*b*][1,4]dioxin-2-ylmethyl) 4-methylbenzenesulfonate (PEDOT-OTs) films yielded a polymeric material that consisted of a redox active disulfide attached to a conducting PEDOT backbone. This dual redox material exhibited impressive cycling stability, on account of the fixation of the DMcT moiety, the electrocatalytic activity of dual redox material, and the conductivity provided by the PEDOT backbone.[36] Nonetheless, these electrodes suffered from a reduced overall capacity, which was attributed to the film thickness, which led to limited accessibility throughout the depth of the film.

Building upon this prior work, this study seeks to introduce a new synthetic approach designed to access nanoscale PEDOT-DMcT-Li dual redox particles. Such an approach aims to address and mitigate inherent limitations associated with bulk hybrid materials like those in the previously discussed work that include less than desirable capacity and cycling stability, both paramount properties in the realm of active materials for battery electrodes. Additionally, the particle architecture enables a straightforward electrode fabrication method where drop-casting of homogenized dispersions is applicable. The improvements gained by synthesizing this active material at the nanoscale are demonstrated through a comprehensive exploration of various cycling methodologies.

RESULT AND DISCUSSION

Synthesis and Characterization of PEDOT-DMcT-Li Nanoparticles. To obtain the PEDOT-DMcT-Li particles it was proposed to first synthesize EDOT particles that could be functionalized with the DMcT. Thus, the tosylated EDOT compound (EDOT-OTs)[36] was synthesized from hydroxymethyl EDOT (EDOT-OH) as the starting monomer for this work. On account of the low solubility of EDOT-OTs, standard emulsion polymerization techniques were not suitable for synthesizing PEDOT-OTs nanoparticles via oxidative polymerization.[37−39] However, a water-free synthesis approach[40] using polyvinylpyrrolidone (PVP) as a surfactant did allow access to PEDOT-OTs nanoparticles (Figure 1a and Scheme S1a, see Experimental Section and Supporting Information for more details). PEDOT-OH nanoparticles were synthesized using EDOT-OH with the same procedure shown in Scheme S1b as a control. The purified PEDOT-OTs nanoparticles are then reacted with lithiated DMcT (DMcT-2Li) to yield PEDOT-DMcT-Li nanoparticles as described in the Experimental Section. The resulting size of the PEDOT-DMcT-Li nanoparticles after drying in a vacuum oven at 55 °C was determined through analysis of the scanning electron microscopy (SEM) image (Figure 1b), which revealed dry PEDOT-DMcT-Li nanoparticles with an average diameter of 107 ± 10 nm. Additionally, dynamic light scattering (DLS) measurements of the PEDOT-DMcT-Li nanoparticles immersed in 1 M lithium bis(trifluoromethanesulfonyl)imide (LiTFSI) in tetraglyme (G4) (electrolyte of choice for electrochemical characterization) indicate that the particles swell to an average diameter of 153 ± 24 nm with a narrow distribution (Figure 1c). The functionalization with lithiated DMcT was confirmed through TGA analysis (Figure S1a), UV-vis-NIR (Figure S1b), and FT-IR (Figure S1c). In the TGA result, a distinctive mass loss was observed in the temperature range of 120−200 °C, which corresponds to the thermal decomposition temperature range for the DMcT

https://doi.org/10.1021/acs.chemmater.4c02387
Chem. Mater. 2024, 36, 9959−9969

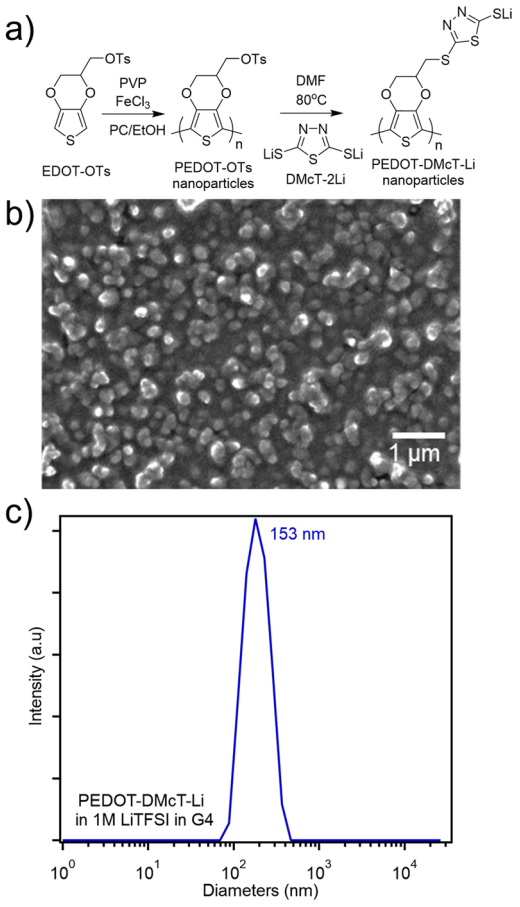

Figure 1. (a) Reaction scheme for the synthesis of PEDOT-DMcT-Li nanoparticles. (b) Scanning electron microscopy (SEM) image of dry PEDOT-DMcT-Li nanoparticles 107 ± 10 nm in diameter. (c) Particle size measured by dynamic light scattering (DLS) in 1 M LiTFSI in a tetraglyme (G4) electrolyte.

moiety.[41] The UV-vis-NIR spectrum of the PEDOT-DMcT-Li nanoparticle dispersion further confirms successful DMcT functionalization, indicated by a characteristic peak at λ = 346 nm corresponding to the DMcT moiety. Using a calibration curve constructed from lithiated DMcT small molecules (Figure S2b), it was determined that approximately half of the mass from PEDOT-DMcT-Li originates from thiolate components consistent with the (near) completion of DMcT functionalization (see Supporting Information for more details). The UV-vis-NIR spectrum on the PEDOT-OTs nanoparticle dispersion (Figure S1b) confirms that they are in the oxidatively *p*-doped state. Notably, the broad absorption bands at $\lambda \gtrsim 800$ nm correspond to the polaronic and bipolaronic states of the oxidized PEDOT backbone, while there is a strong absorption band at 489 nm for the neutral PEDOT backbone.[42] Additionally, a notable reduction in the oxidative p-doped state of the final PEDOT-DMcT-Li nanoparticles, compared with the starting PEDOT-OTs nanoparticles, was observed. This reduction is evidenced by a weaker polaron absorption band at $\lambda \gtrsim 800$ nm, suggesting significant removal of residual iron.

Electrochemical Properties PEDOT-DMcT-Li Nanoparticles. To explore the accessible electrochemical reactions in the dual redox PEDOT-DMcT-Li nanoparticles, cyclic voltammetry (CV) of PEDOT-DMcT-Li was performed with particles coated on carbon paper (CP) as the working electrode. CV of PEDOT-DMcT-Li revealed a strong disulfide redox couple in the region anticipated for DMcT at 3.6 V for thiolate oxidation and 3 V for disulfide reduction vs Li/Li^+ (Figure S3a). Additional peaks can be deconvoluted to peaks observed in the PEDOT backbone at approximately 3.3 V during oxidation and 2.5 V during reduction (Figure S3b). The CV experiment was also performed in a lithium coin cell with PEDOT-DMcT-Li nanoparticles as the cathode electrode. In short, cathodes were prepared as follows: nanoparticles were sonicated in dimethylformamide (DMF) overnight with poly(vinylidene fluoride) (PVDF) binder and carbon black (CB) at a PEDOT-DMcT-Li:CB:PVDF ratio of 90:5:5 wt %, resulting in a homogeneous dispersion. The dispersion was then drop-cast onto CP and dried to yield the cathode electrode assembly (Figure S4a and S4b). The cathode composition of 90:5:5 wt % PEDOT-DMcT-Li:CB:PVDF was selected to maximize the redox-active nanoparticle mass, with sufficient CB for electronic conduction and PVDF as a polymer binder to ensure good adhesion between the redox-active nanoparticle and the current collector, thereby preventing detachment from the electrode. Carbon paper was selected as the cathode substrate as a prior study revealed that carbon paper allows for favorable electrochemical reversibility for disulfide redox molecules.[43] The PEDOT-DMcT-Li electrode was then assembled into a coin cell in a half-cell configuration versus a lithium foil anode with 1 M LiTFSI in tetraglyme (G4) as the electrolyte. G4 was selected as it has been shown to be stable with lithium metal and disulfide redox species.[44]

The cyclic voltammetry (CV) experiment was carried out on the coin cell held at 45 °C at a slow scan rate of 0.1 mV/s to clearly discern the accessible electrochemical redox reactions (Figure 2b). During the forward scan from 2.0 to 4.0 V vs Li/Li^+, three oxidation peaks were observed. The first peak at $E_{p,Ox1}$ at 2.8 V vs Li/Li^+ corresponds to the oxidation of the PEDOT backbone to form polarons (hole/radical pairs), the second peak at $E_{p,Ox2}$ = 3.1 V vs Li/Li^+ corresponds to the oxidation of thiolate to disulfide, and the third peak at $E_{p,Ox3}$ = 3.7 V vs Li/Li^+ corresponds to further oxidation of PEDOT backbone to form bipolarons (hole/hole pairs) (Figure 2a).[45] During the reverse scan from 4.0 to 2.0 V vs Li/Li^+, only two reduction peak potentials were observed (Figure 2b). The reduction peak at 2.9 V vs Li/Li^+ ($E_{p,Red2}$) coincides with the reduction of disulfide to thiolates and the following reduction peak at 2.6 V vs Li/Li^+ ($E_{p,Red1}$) coincides with the reduction of polaronic PEDOT to neutral PEDOT. Of note is the lack of a clear reduction peak at high potential relating to the conversion of bipolaronic charges back to polaronic charge (Ox3 → Red3). It is possible that the charge compensation of bipolarons with $TFSI^-$ anions stabilizes and thus traps the hole charge carriers, making them inaccessible to reduction. Such a phenomenon has been observed in PEDOT and other thiophene-based conjugated polymers with bipolarons.[46−50] Overall, the redox peaks from the CV experiments provide clear evidence of the successful attachment of thiolate moieties to the PEDOT backbone and demonstrate the reversible dual redox behavior of PEDOT-DMcT-Li.

Galvanostatic Cycling of Li Metal Half Cells with PEDOT-DMcT-Li Cathodes. Room temperature (RT) galvanostatic cycling was performed at a low current density (i) of 0.017 mA/cm^2 (0.05C) to determine the charge and discharge profiles and the accessible capacity. The coin cells consist of PEDOT-DMcT-Li as cathode material and were

https://doi.org/10.1021/acs.chemmater.4c02387
Chem. Mater. 2024, 36, 9959−9969

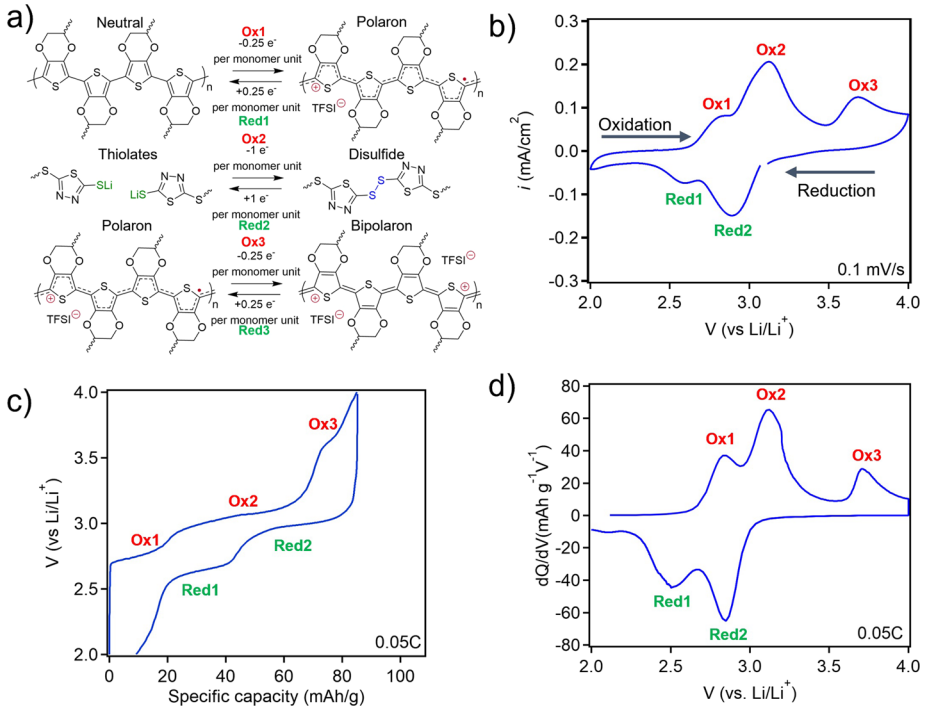

Figure 2. (a) Electrochemical reactions of dual redox PEDOT-DMcT-Li during charge/discharge, consisting of a thiadiazole disulfide/thiolates redox center and an electronically conductive redox active PEDOT backbone. (b) CV of PEDOT-DMcT-Li in a coin cell at 45 °C, 1 M LiTFSI in G4 as the electrolyte, Celgard 2325 as the separator, 0.1 mV/s scan rate. (c) Representative charge−discharge curve of galvanostatic cycling and (d) differential capacity (dQ/dV) plot of PEDOT-DMcT-Li particles at 0.05C.

fabricated in the same procedure as described above. The applied i is determined using the highest possible theoretical capacity of PEDOT-DMcT-Li, which is calculated to be 129.7 mAh/g. This is based on the PEDOT-DMcT-Li particles exhibiting 1.5 electrons reaction per monomer unit, accounting for a one-electron oxidation of the thiolate to form a disulfide and a half-electron contribution due to the oxidation of the PEDOT backbone to yield a polaron and bipolaron (Figure 2a). Figure 2c shows the representative charge/discharge cycling profiles with potential limits of 2 to 4 V vs Li/Li$^+$. The observed charging and discharge potential plateaus are consistent with the redox peaks from the CV measurements. To emphasize this point, Figure 2d replots the galvanostatic cycling in the form of a differential capacity (dQ/dV) plot, which clearly shows that the oxidation potentials align well with coin cell CV data presented in Figure 2b. The dQ/dV plot further demonstrates the absence of the Red3 peak (Figure 2d), highlighting the presence of trapping of bipolaronic charge during reductive discharge.

Considering that PEDOT is a p-type semiconductor, the oxidation and reduction of PEDOT through electrochemical doping can modulate the electronic conductivity of the PEDOT-DMcT-Li nanoparticles during cell cycling. To further probe the change of conductivity, electrochemical impedance spectroscopy (EIS) measurements were performed on the Li/PEDOT-DMcT-Li cell. Specifically, the cell was cycled at a rate of 0.1C (0.034 mA/g) for 15 min, followed by EIS measurements, and then cycling was resumed until the predefined potential limits for charging and discharging were reached. Figure 3a shows the representative Nyquist plots of the cell before the charging cycle (2.2 V), at the end of the charging cycle (4.0 V), and at the end of the discharging cycle (2.0 V). The cell has the highest impedance at 2.2 V; then the

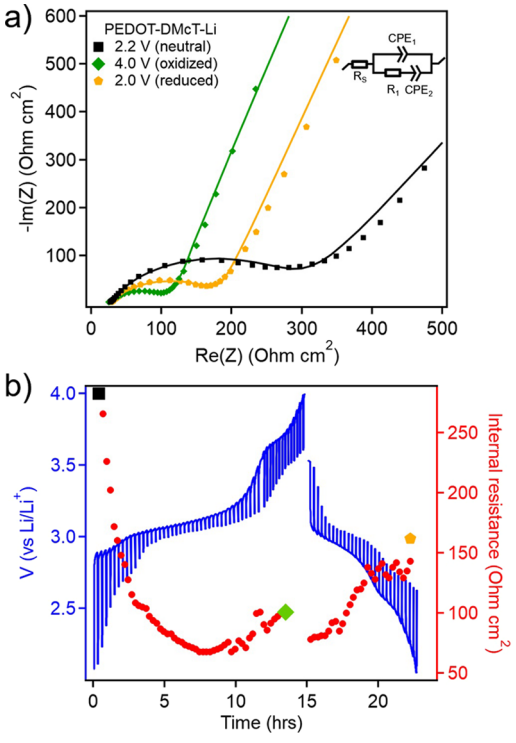

Figure 3. (a) Nyquist plots from Li/PEDOT-DMcT-Li coin cells prior to charging (2.2 V), after charging (4.0 V), and after discharge (2.0 V). (b) Charge/discharge cycling of PEDOT-DMcT-Li at 0.1C at 15 min intervals and the corresponding internal electrode resistance from EIS measurements at each interval. The black square represents the neutral state (2.2 V), green diamond represents the charged state (4.0 V), and orange pentagon represents the discharged state (2.0 V) of the PEDOT-DMcT-Li cathode.

https://doi.org/10.1021/acs.chemmater.4c02387
Chem. Mater. 2024, 36, 9959−9969

cell impedance decreases at 4.0 V and increases again at 2.0 V. These changes in impedance can result only from the variation in the electronic conductivity PEDOT-DMcT-Li.

An equivalent circuit (shown in Figure 3a) was used to fit the experimental impedance spectra to provide a more granular quantification of the electrode resistance as a function of potential during charging and discharging. In the circuit, R_S is series resistance at high frequency due to resistance from the electrolyte solution, wires, and contacts; the parallel combination R_1 and CPE_1 (constant phase element) is the total resistance and nonideal capacitance, respectively, from the electrode, and CPE_2 models low frequency capacitive behavior.[51,52] The extracted R_1 values (internal electrode resistance) are plotted and superimposed on the charge/discharge profile in Figure 3b. Prior to the charging cycle, R_1 was 282 $\Omega \cdot cm^2$ at 2.2 V. Upon charging, there was a monotonic decrease in R_1 until reaching a local minimum at 3.1 V (R_1 = 67 $\Omega \cdot cm^2$) arising from the oxidation of the PEDOT backbone to form polarons. Upon further oxidation, an increase in R_1 was observed until reaching the charging potential limit of 4 V where R_1 = 101 $\Omega \cdot cm^2$. This observation suggests that at higher voltages, the conductivity of the PEDOT-DMcT-Li cathode initially increases and then decreases, a trend similarly reported in several other organic semiconductors, due to lower mobility of bipolaron compared to polaron.[53−55] Upon reduction by discharging to 2.2 V, R_1 increased back to 163 $\Omega \cdot cm^2$ as the PEDOT backbone is reduced. Note that R_1 does not increase to the initial higher value, suggesting the PEDOT does not return to the fully neutral state upon discharge.

When using dual-redox organic electrodes materials, self-discharge is possible on account of intermolecular electron transfer between redox centers.[56−61] To determine the extent of self-discharge, PEDOT-DMcT-Li coin cells were galvanostatically charged to 4.0 V and then allowed to rest at open circuit, as shown in Figure S5. The initial drop and subsequent stabilization in voltage are attributed to the dissipation of cell polarization from electrode overpotentials and salt concentration gradients established from the galvanostatic charging. Notably, after stabilization, PEDOT-DMcT-Li electrodes overall demonstrated exceptional stability with minimal self-discharge. Voltage measurements recorded at 3.44 V after 1 day of rest, when plotted against the representative charge−discharge curve, showed that the cell retained over 99.7% of its initial specific discharge capacity (SDC). However, at the end of a seven-day monitoring period, the OCV measured 3.28 V, indicating a slightly reduced but still commendable SDC retention of 98.8%. This performance stands in contrast to batteries incorporating other polymer-based electrodes, which exhibited an approximate 1% daily decrease in specific capacity due to noticeable self-discharge.[62]

Rate Dependence Cycling of PEDOT-DMcT-Li and PEDOT-OH Nanoparticles. To assess the cycling rate capability, lithium half cells equipped with PEDOT-DMcT-Li and PEDOT-OH nanoparticle cathodes were cycled at room temperature at rates ranging from 0.05C to 1C. Following this, the cells were returned to 0.1C and 0.05C to evaluate the stability of their accessible capacity during extended, sequential C-rate cycling (Figures 4a). During these cycles, both the specific charge capacity (SCC) and the specific discharge capacity (SDC) were recorded. For PEDOT-DMcT-Li, an SDC of 69.5 mAh/g is achieved (53.6% of maximum theoretical capacity) at 0.05C (6.5 mA/g), while at 1C

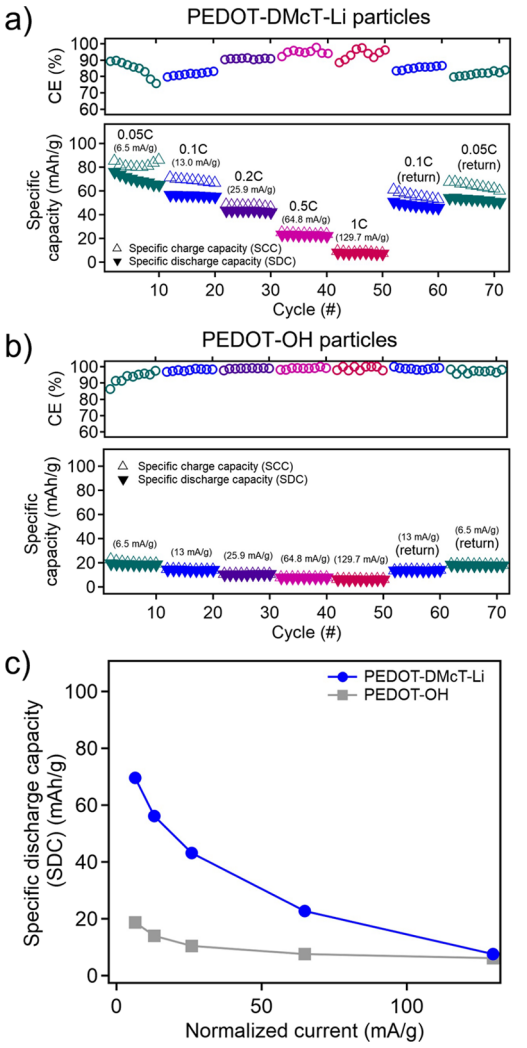

Figure 4. (a) Coulombic efficiency (CE) and specific capacities at various C-rates for PEDOT-DMcT-Li and (b) PEDOT-OH cycled at the same gravimetric current density (mAh/g) based on the theoretical capacity of PEDOT-DMcT-Li. (c) Modified Peukert plot of PEDOT-DMcT-Li and PEDOT-OH with specific discharge capacity (SDC) at different gravimetric current densities (normalized current) .

(129.5 mA/g), an SDC of only 7.6 mAh/g is achieved (5.9% of maximum theoretical capacity). Additionally, CE data are also included in the upper graphs of Figure 4a and 4b to evaluate the effectiveness of the cycling process, which is defined as the SDC divided by the SCC. At the lower C-rate of 0.05C, the PEDOT-DMcT-Li has CE of 80.0% which improves to a CE of 93.8% at 1C.

To distinguish the specific impact of the PEDOT backbone and disulfide components, cathodes consisting of PEDOT-OH nanoparticles were assembled as a comparison (Figure 4b). When cycling at the same gravimetric current density as PEDOT-DMcT-Li, PEDOT-OH achieves an SDC of 18.7 mAh/g at 0.05C (6.5 mA/g) and an SDC of 6.2 mAh/g at 1C (129.5 mA/g). As depicted in Figure 4c, a modified Peukert plot illustrates the SDC of PEDOT-DMcT-Li and PEDOT-OH with gravimetric current density, indicating that the majority of capacity in the PEDOT-DMcT-Li system is coming from disulfides at lower rates, whereas at higher rates, the majority of capacity is coming from the PEDOT backbone.

https://doi.org/10.1021/acs.chemmater.4c02387
Chem. Mater. 2024, 36, 9959−9969

While bipolaron charging and discharging plateaus were indeed observed at very slow cycling rates for PEDOT-DMcT-Li nanoparticles, specifically at rates of 0.2C and below (Figure S6), PEDOT is known to be challenging to charge to a fully bipolaron state.[63] As shown in Figure S7, PEDOT-OH demonstrated a more capacitive behavior with no clear observation of the bipolaron charging plateau. The fact that a bipolaron can be formed and accessed in PEDOT-DMcT-Li nanoparticles is likely due to the increased swelling of PEDOT-DMcT-Li in LiTFSI/G4 electrode compared to PEDOT-OH (swollen particle size of 153 nm (Figure 1c) vs 138 nm (Figure S8), respectively). A control study of PEDOT-OH cycled at various C-rates was used to examine the accessibility of the PEDOT backbone, where the C-rates were determined based on the theoretical capacity of PEDOT-OH assuming 0.25 e^- per EDOT unit (only forming polaron) rather than being set at the same current density as PEDOT-DMcT-Li. At 0.05C, the highest capacity achieved was 31.8 mAh/g (Figure S9), which is notably closer to the theoretical capacity of PEDOT-OH forming only polarons (theoretical specific capacity of 39.0 mAh/g) than when assuming the formation of bipolarons (theoretical capacity of 77.9 mAh/g). Therefore, it is reasonable to conclude that the theoretical specific capacity for PEDOT-DMcT-Li nanoparticles is 108.1 mAh/g for the case where PEDOT only forms polarons (Table S1).

Charge−Discharge Optimization via Asymmetric Cycling Rate Conditions. The charge−discharge data shown previously reveal a gap between the measured SCC and SDC, as indicated by CE, in the range of 80−90%. Of the multiple potential sources of this phenomenon, one possible cause is the difference in reaction rates associated with the charging (oxidation) and discharging (reduction) of PEDOT-DMcT-Li particles. Differences in the relative ease of charging and discharge of redox-active materials are acknowledged phenomena that are known to impact different battery electrode chemistries.[64−66] In order to probe this behavior, CV sweeps were examined to determine the difference between the amount of charge transferred in and out of PEDOT-DMcT-Li nanoparticles over a fixed potential window and a constant scan rate (Figures 2b and S10a). Total charge transferred during the half sweep was determined by integrating the CV peaks: three oxidation peaks at 2.8 V: 0.076 C/cm^2 (11%), 3.1 V: 0.517 C/cm^2 (72%), and 3.7 V: 0.012 C/cm^2 (17%) (Figure S10e) and two reduction peaks at 2.6 V: 0.109 C/cm^2 (23%) and 2.9 V: 0.360 C/cm^2 (77%) (Figure S10f). Integration of these peaks reveals that the amount of disulfides reduced during the return sweep is less than the amount of thiolates initially oxidized. A reasonable hypothesis for the cause of this observation is charge trapping within the particle core due to reduced electronic conductivity at the particle surfaces after discharge (Scheme S2). This observation aligns with the data discussed in Figure 3b, which shows that the resistance R_1 at 2 V after discharge is lower than R_1 at 2.2 V before cycling. This indicates that due to charge trapping the electronic conductivity of the PEDOT-DMcT-Li nanoparticles does not return to its original state after cycling. Similar behavior can be observed in other semiconducting polymer systems. S.H. Oh and co-workers reported using polythiophene as an electroactive species, and they attributed the relatively low utilization of the battery capacity to the change in the conductivity of the conducting polymer.[67] Charging (oxidation) converts polythiophene to a conductive state, aiding further charge transfer, while discharging (reduction) converts doped polythiophene to a nonconductive state near the current collector interface, limiting electronic access to the interior of the particles.

A second approach to address the issue of the difference in rate controlled accessible capacity in a battery assembly is to increase the overall time allowed for discharge relative to charging time. With a slower discharge rate, a greater extraction of overall energy is possible before the electrode reaches a "fully discharged" state, as defined by a prescribed lower voltage threshold. To test this hypothesis, PEDOT-DMcT-Li half-cells were prepared in an identical fashion and cycled using asymmetric rates, with the discharging rate being half that of the charging rate (e.g., 1C charging followed by 0.5C discharging), the results of which are shown in Figures 5a. At slower charging rates, the discharge capacity of the half-

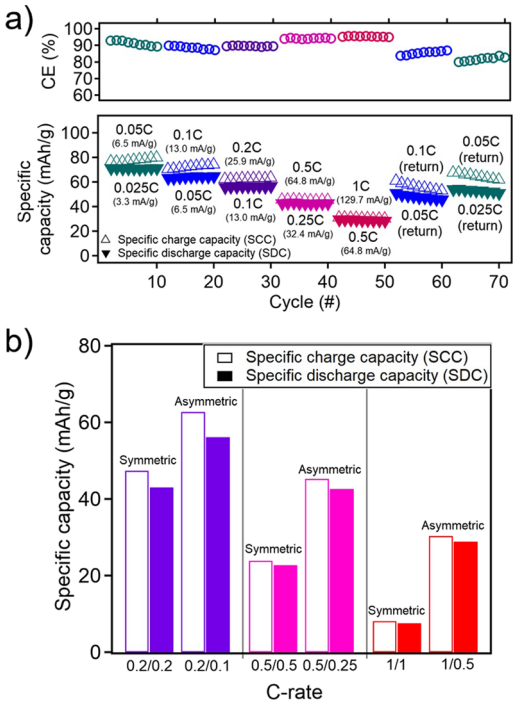

Figure 5. (a) Coulombic efficiency (CE) and specific capacity at asymmetric charge/discharge cycling rates of PEDOT-DMcT-Li at room temperature (2× slower discharging). (b) Comparison of SCC and SDC of PEDOT-DMcT-Li at symmetric cycling and asymmetric cycling (2× slower discharging) for the higher rate regime.

cell showed modest improvement, but the CE was significantly higher (91% with asymmetric cycling vs 80% with symmetric cycling for a 0.05C charge rate). Moreover, sequential asymmetric cycling allows for greater SCC at higher C-rates compared with symmetric cycling. Consequently, a greater SDC is achievable in the higher rate regime. For example, at a 1C charge rate, an SDC of 29.0 mAh/g was observed for asymmetric cycling compared to 7.6 mAh/g for symmetric cycling (Figure 5b). Overall, asymmetric cycling provides a pathway to address the differences in charge and discharge kinetics, leading to enhanced accessible capacity and CE.

The impact of asymmetric charging on the cycling stability of PEDOT-DMcT-Li was also tested. Half-cells were subjected to 400 cycles of galvanostatic charging at a charging rate of 0.1C with either 0.1C or 0.05C discharge rates (Figure 6). At 100 cycles, the SDC of PEDOT-DMcT-Li cycled with symmetric charging conditions showed an SCC of 60.7

https://doi.org/10.1021/acs.chemmater.4c02387
Chem. Mater. 2024, 36, 9959−9969

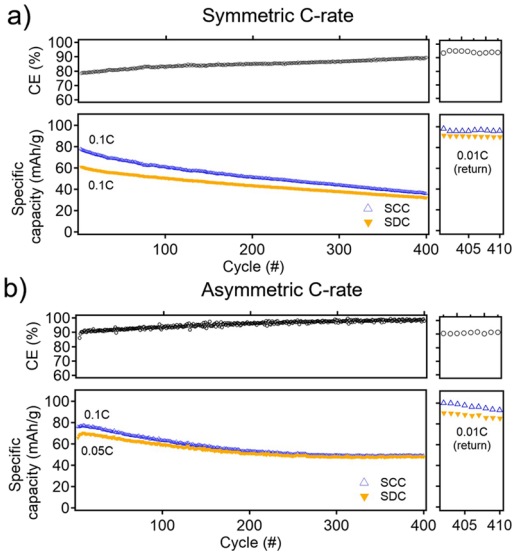

Figure 6. Long-term cycling Coulombic efficiency (CE), specific charge capacity (SCC), and specific discharge capacity (SDC) of PEDOT-DMcT-Li (a) at symmetric rate cycling at 0.1C for 400 cycles then return to 0.01C for 10 cycles and (**b**) the corresponding asymmetric rate cycling condition, 0.1C for charging and 0.05C for discharging across 400 cycles then return to 0.01C for 10 cycles.

mAh/g and an SDC of 51.2 mAh/g, and that with asymmetric cycling showed an SCC of 63.0 mAh/g and an SDC of 58.8 mAh/g, both of which reach 84% capacity retention relative to their SDC on the first cycle. At 400 cycles, PEDOT-DMcT-Li cycled with symmetric charging conditions showed an SCC of 35.6 mAh/g and an SDC of 31.8 mAh/g (52% capacity retention). In contrast, the one cycled under asymmetric conditions maintained an SCC of 48.8 mAh/g and an SDC of 47.7 mAh/g (69% capacity retention). Making this more impressive, the samples cycled under asymmetric charging conditions exhibited a much higher CE across the lifetime of the cycling experiment (94.7% vs 78.7% at 100 cycles and 98.2% vs 90.6% at 400 cycles), indicating less charge trapping when the asymmetric cycling rate method was adopted. As a final observation, the deeper discharging of the PEDOT-DMcT-Li material with a reduced discharge rate does not appear to impact the ability of the half-cell to recover most of their capacity when returned to a significantly lower C-rate of 0.01C. The half-cell that underwent asymmetric C-rate cycling achieved an SDC of 88.0 mAh/g, with a CE of 91.5%. Similarly, the half-cell cycled at a symmetric C-rate exhibited an SDC of 90.6 mAh/g with a CE of 94%. Both conditions show a nearly complete recovery compared to the freshly prepared half-cell cycled at 0.01C (SDC of 91.9 mAh/g and CE of 90.0%) (Figure S11). The achievable SCC and SDC are very close to the theoretical capacity of PEDOT-DMcT-Li, assuming only polarons form on the PEDOT backbone (108.1 mAh/g). Collectively, these findings underscore that the active material experiences minimal degradation over 400 cycles. The gradual decline in capacity is primarily attributed to charge trapping phenomena occurring within the PEDOT-DMcT-Li dual redox materials, a challenge for which the initial optimization steps have been shown in this work.

CONCLUSION

In conclusion, the research presented describes the development of organic cathode materials for Li-ion batteries, using nanosized conjugated PEDOT polymer particles with dense, redox-active disulfide cross-links. Through detailed CV and galvanostatic cycling experiments, it was possible to isolate the distinct contributions of the various redox components, namely, the redox responsive DMcT disulfide/thiolate redox couple and PEDOT. Moreover, EIS measurements on the Li/PEDOT-DMcT-Li cell show that changes in impedance during cycling are directly related to the variation in electronic conductivity of the PEDOT-DMcT-Li nanoparticles and thus can influence rate dependent charge/discharge cycling. At low C-rates, battery cycling tests revealed that these PEDOT-DMcT-Li dual redox materials demonstrate excellent specific capacities—achieving 91.9 mAh/g (85% of theoretical maximum capacity, using only polaron access for PEDOT). Importantly, PEDOT-DMcT-Li electrodes exhibited minimal self-discharge, maintaining a 98.8% capacity after 7 days.

Asymmetric rate cycling was explored to address the observed charge trapping caused by the difference in the reaction rates between the charging (oxidation) and discharging (reduction) of PEDOT-DMcT-Li particles. Specifically, using asymmetric cycling—where the discharge rate is two times slower than the charge rate—improved the specific discharge capacity (SDC) and significantly increased the Coulombic Efficiency (CE) to 91% at 0.05C, compared to 80% with symmetric cycling. At higher C-rates, asymmetric cycling conditions led to a dramatic increase in SDC to 29.0 mAh/g compared to just 7.6 mAh/g under conventional symmetric cycling. This method of asymmetric cycling addresses disparities in charge and discharge kinetics, resulting in improved accessible capacity and CE. Long-term cycling stability tests further showed that capacity retention was primarily due to charge trapping rather than material degradation, as evidenced by capacity recovery after 400 cycles. Notably, asymmetric cycling achieved 69% discharge capacity retention compared to 52% under symmetric conditions. Overall, this work demonstrates a promising approach for designing, testing, and operating dual redox polymers as cathode materials, enabling high capacities and improved rate capabilities in organic batteries.

EXPERIMENTAL SECTION

Materials. Dimethyl sulfoxide, anhydrous, ≥99.9%, p-toluenesulfonyl chloride, ReagentPlus, ≥99%, lithium hydroxide, reagent grade, 98%, propylene carbonate, ReagentPlus, 99%, hydroxymethyl EDOT, 95%, and chloroform-d (99.8 atom % D, contains 0.03 % v/v TMS), were from Sigma-Aldrich. Spectra Por S/P 1 Dialysis Membrane Trial Kit, 6000−8000 Da, 32 mm Flat Width, was from Cole-Parmer.

Synthesis and Characterization of EDOT-OTs. 2,3-Dihydrothieno[3,4-*b*][1,4]dioxin-2-ylmethyl 4-methylbenzenesulfonate (EDOT-OTs) was synthesized with a method modified from Rodríguez-Calero et al.[36] 2,3-Dihydrothieno[3,4-*b*][1,4]dioxin-2-yl)-methanol (EDOT-OH) monomer was purchased and used as-is. EDOT-OH:^{1}H NMR (400 MHz, $CDCl_3$) δ 6.35 (dd, 2H, S−CH), 4.30−4.05 (m, 3H, O−CH2−CH−O), 3.95−3.78 (m, 2H, CH2), 1.84 (t, 1H, −OH). ^{13}C NMR (400 MHz, $CDCl_3$) δ 141.4, 99.8, 74.0, 65.7, 61.6.

A solution of 5 g (29.0 mmol) of EDOT-OH, triethylamine (TEA) (4.4 g, 6.06 mL, 43.4 mmol), and 4-dimethylaminopyridine (DMAP) (11 g, 90.0 mmol) in 25 mL of dichloromethane was maintained at 0 °C by an ice bath. To this solution was added p-toluenesulfonyl chloride (TsCl) (12.15 g, 63.7 mmol) incrementally, and the reaction mixture was stirred and allowed to warm to room temperature overnight. The organic layer was washed with DI water three times and then dried with anhydrous $MgSO_4$. The organic layer was concentrated by rotary evaporation. The resulting tosylated EDOT

https://doi.org/10.1021/acs.chemmater.4c02387
Chem. Mater. 2024, 36, 9959−9969

(EDOT-OTs) was purified via flash chromatography. The column was run with pure hexane, 10% DCM in hexane, 30% DCM in hexane, and finally 50% DCM in hexane for 10 column volumes each. The resulting EDOT-OTs were concentrated by rotary evaporation followed by a vacuum. 8.16 g of EDOT-OTs was obtained in a yield of 86.3%. EDOT-OTs: ^{1}H NMR (400 MHz, $CDCl_3$) δ 7.8 (d, 2H), 7.37(d, 2H), 6.32 (d, 1H), 6.26 (d, 1H), 4.36 (m, 1H), 4.20 (m, 3H), 4.03 (d, 1H), 2.46 (s, 3H). ^{13}C NMR (400 MHz, $CDCl_3$) δ: 145.3, 140.9, 140.3, 132.4, 130.0, 128.0, 100.3, 70.8, 66.9, 65.0, 21.7.

Synthesis of PEDOT-OTs Particles. A 2 g portion of PVP was dissolved in 300 mL of ethanol. To the solution was added 1 g of EDOT-OTs dissolved in 100 mL of propylene carbonate (PC). The solution was stirred at 800 rpm for 15 min. A total of 7 g of anhydrous iron(III) chloride was added, and the reaction was carried out for 1 day. The mixture turned into a yellow-green dispersion. The result particle dispersion was concentrated by rotary evaporation and then transferred to a Spectra Por S/P 1 dialysis membrane, 6−8 kDa. The dialysis membrane was then placed in 3.5 L of methanol. Methanol was replaced 2 times a day for 4 days. The PEDOT-OTs particle dispersion was then concentrated by rotary evaporation and dried under a vacuum for 2 days.

Synthesis of PEDOT-OH Particles. PEDOT-OH particles were synthesized by the same procedure as described above. Instead of the EDOT-OTs monomer, hydroxymethyl EDOT was used. A total of 0.8 g of PVP was dissolved in 120 mL of ethanol. To the solution was added 400 mg of EDOT-OH dissolved in 40 mL of PC. The solution was stirred at 800 rpm for 15 min. A total of 2.8 g of anhydrous iron(III) chloride was added, and the reaction was carried out for 1 day. The mixture turned into a yellow-green dispersion. The resulting particle dispersion was concentrated by rotary evaporation and then transferred to a Spectra Por S/P 1 dialysis membrane of 6−8 kDa. The dialysis membrane was then placed in 3.5 L of methanol. Methanol was replaced 2 times a day for 4 days. The PEDOT-OH particles dispersion was then concentrated by rotary evaporation and then dried under a vacuum for 2 days.

DMcT-2Li. DMcT (21.18 g, 140.9 mmol) and LiOH (6.749 g, 281.8 mmol) were dissolved in ethanol. The resulting solution was stirred at 300 rpm for 1 day. The solution was dried by rotary evaporation and then under a vacuum.

Synthesis of PEDOT-DMcT-Li. PEDOT-OTs (340 mg) was dispersed with 0.5 M of DMcT-2Li in DMF solution via bath sonication. The resulting dispersion was heated at 90 °C for 24 h. The resulting particles were concentrated by rotary evaporation and then transferred to a Spectra Por S/P 1 dialysis membrane, 6−8 kDa. The dialysis membrane was then placed in 3.5 L of methanol. Methanol was replaced 2 times a day for 4 days. PEDOT-DMcT-Li particle dispersion was then concentrated by rotary evaporation and then dried under vacuum for 2 days.

UV-Vis-NIR Spectroscopy. The Shimadzu UV-3600 Plus UV-vis-NIR spectrophotometer was employed to conduct measurements ranging from 280 to 1650 nm, with a sampling interval of 1 nm. DMF was utilized as the supporting solvent for all sample solutions or dispersions. Particle characterization was performed using 0.05 mg/mL particle suspensions.

Scanning Electron Microscopy (SEM). For bare particles, a silicon substrate was sectioned into 1 cm × 1 cm squares and underwent a thorough cleaning process involving sonication in acetone followed by methanol. Subsequently, 50 μL of a 0.3 mg/mL particle dispersion in water was deposited onto the silicon substrates and left to dry on an 80C hot plate. Silicon substrates with polymer particles were adhered to the SEM mounts. Cathodes with polymer active material were adhered onto SEM mounts with conductive copper tape. Prior to SEM imaging, 8 nm of platinum/palladium was coated onto samples with a sputter coater (Cressington 208HR sputter coater). Carl Zeiss Merlin SEM, a high-resolution Field Emission Scanning Electron Microscope (FE-SEM), was used to analyze all samples using a 3 kV beam voltage. Twenty particles were averaged to obtain the average diameters for particles

Thermogravimetric Analysis (TGA). TGA was performed by using a TA Instruments Discovery TGA 5500 at a rate of 10 °C/min. Samples were predried in a vacuum oven at 55 °C overnight to remove residual water.

Cathodes Fabrication of Polymer Active Material. Polymer particle active material cathodes were fabricated using Sigracet GDL 39 AA carbon paper, which was cut into 0.5 in. round substrates using a paper punch. The substrates were then placed on a flat Teflon sheet for casting. Cathode suspensions were prepared in DMF with 5 mg/mL of PVDF (polyvinylidene fluoride) and 5 mg/mL of CB (carbon black) to achieve a total solids concentration of 100 mg/mL, while the ratios of active material, carbon black, and PVDF were kept at 90:5:5 by weight. The suspensions were homogenized overnight by using a bath sonicator. Once cast onto the carbon paper substrates, the samples were dried in a vacuum oven at 55 °C overnight before being transferred into an argon glovebox for coin cell fabrication as described below.

Coin Cell Fabrication. Coin cells (size 2032) were assembled using polished Li foil punched into 12 mm circles (1.13 cm^2 in area). A total of 90 μL of electrolyte (1 M LiTFSI in G4) was applied in three separate aliquots of 30 μL each, one atop each of the Li foils, a Celgard 2325 separator, and the cathode layer. The cells were crimped using an MTI Corporation MSK-110 crimper to a pressure of 600 psi (approximately 42 kg/cm^2). Subsequently, the coin cells were equilibrated overnight to fully equilibrate. Finally, the cells were examined using electrochemical impedance spectroscopy (EIS) to detect any instances of shorting or other irregularities prior to cycling.

Galvanostatic Cycling (GC). GC experiments were conducted utilizing a Neware CT-4008T-5 V50 mA eight-channel battery cycler. Coin cells were positioned in 2032 cell holders with lead wires soldered to the terminals and insulated by using fiberglass felt pockets to mitigate abrupt temperature fluctuations. For elevated temperature cycling, a Neware 25L temperature chamber was used.

■ ASSOCIATED CONTENT

Supporting Information

The Supporting Information is available free of charge at https://pubs.acs.org/doi/10.1021/acs.chemmater.4c02387.

Synthesis of PEDOT-DMcT-Li and PEDOT-OH particles, thermogravimetric analysis (TGA) and UV-vis-NIR and FT-IR of PEDOT particles, UV-vis-NIR absorbance of DMcT-2Li in DMF and calibration curve of peak absorbance, CV of PEDOT-DMcT-Li and PEDOT-OH, SEM images of PEDOT-DMcT-Li and PEDOT-OH particles on the electrode, self-discharge test of PEDOT-DMcT-Li, representative charge−discharge curves of PEDOT-DMcT-Li, representative charge−discharge curves of PEDOT-OH, dynamic light scattering (DLS) of PEDOT-OH particles, Coulombic efficiency and capacity at various C-rates and current density for PEDOT-OH, theoretical capacity calculation for PEDOT-DMcT-Li and PEDOT-OH and PEDOT-DMcT-Li, coin cell CV and integration of PEDOT-DMcT-Li in the coin cell at RT and 45C, charge trapping within the conjugated polymer schematic, and lower C rate cycling of PEDOT-DMcT-Li at 0.01C (PDF)

■ AUTHOR INFORMATION

Corresponding Authors

Stuart J. Rowan − *Pritzker School of Molecular Engineering and Department of Chemistry, University of Chicago, Chicago, Illinois 60637, United States; Joint Center for Energy Storage Research and Chemical Sciences and Engineering Division, Argonne National Laboratory, Argonne, Illinois 60439, United States;* orcid.org/0000-0001-8176-0594; Email: stuartrowan@uchicago.edu

https://doi.org/10.1021/acs.chemmater.4c02387
Chem. Mater. 2024, 36, 9959−9969

Shrayesh N. Patel − *Pritzker School of Molecular Engineering, University of Chicago, Chicago, Illinois 60637, United States; Joint Center for Energy Storage Research and Chemical Sciences and Engineering Division, Argonne National Laboratory, Argonne, Illinois 60439, United States;* orcid.org/0000-0003-3657-827X; Email: shrayesh@uchicago.edu

Authors

Hongyi Zhang − *Pritzker School of Molecular Engineering, University of Chicago, Chicago, Illinois 60637, United States; Joint Center for Energy Storage Research, Argonne National Laboratory, Argonne, Illinois 60439, United States*

Garrett L. Grocke − *Pritzker School of Molecular Engineering, University of Chicago, Chicago, Illinois 60637, United States; Joint Center for Energy Storage Research, Argonne National Laboratory, Argonne, Illinois 60439, United States;* orcid.org/0000-0001-8661-5038

George Rose − *Pritzker School of Molecular Engineering, University of Chicago, Chicago, Illinois 60637, United States*

Complete contact information is available at: https://pubs.acs.org/10.1021/acs.chemmater.4c02387

Notes

The authors declare no competing financial interest.

■ ACKNOWLEDGMENTS

The authors gratefully acknowledge financial support from the Joint Center for Energy Storage Research (JCESR), an Energy Innovation Hub funded by the U.S. Department of Energy, Office of Science, Basic Energy Sciences (BES). This work made use of the shared facilities at the University of Chicago Materials Research Science and Engineering Center, supported by the National Science Foundation under Award Number DMR-2011854. Parts of this work were carried out at the Soft Matter Characterization Facility of the University of Chicago.

■ REFERENCES

(1) Ambrose, H.; Kendall, A. Understanding the Future of Lithium: Part 1. *Resource Model. J. Ind. Ecol.* **2020**, *24* (1), 80−89.
(2) Wanger, T. C. The Lithium Future-Resources, Recycling, and the Environment. *Conserv. Lett.* **2011**, *4* (3), 202−206.
(3) Kwon, G.; Ko, Y.; Kim, Y.; Kim, K.; Kang, K. Versatile Redox-Active Organic Materials for Rechargeable Energy Storage. *Acc. Chem. Res.* **2021**, *54* (23), 4423−4433.
(4) Nakahara, K.; Iwasa, S.; Satoh, M.; Morioka, Y.; Iriyama, J.; Suguro, M.; Hasegawa, E. Rechargeable Batteries with Organic Radical Cathodes. *Chem. Phys. Lett.* **2002**, *359* (5−6), 351−354.
(5) Leedy, D. W.; Muck, D. L. Cathodic Reduction of Phthalimide Systems in Nonaqueous Solutions. *J. Am. Chem. Soc.* **1971**, *93* (17), 4264−4270.
(6) Zhan, L.; Song, Z.; Shan, N.; Zhang, J.; Tang, J.; Zhan, H.; Zhou, Y.; Li, Z.; Zhan, C. Poly(Tetrahydrobenzodithiophene): High Discharge Specific Capacity as Cathode Material for Lithium Batteries. *J. Power Sources* **2009**, *193* (2), 859−863.
(7) Zhan, L.; Song, Z.; Zhang, J.; Tang, J.; Zhan, H.; Zhou, Y.; Zhan, C. PEDOT: Cathode Active Material with High Specific Capacity in Novel Electrolyte System. *Electrochim. Acta* **2008**, *53* (28), 8319−8323.
(8) Deng, S.-R.; Kong, L.-B.; Hu, G.-Q.; Wu, T.; Li, D.; Zhou, Y.-H.; Li, Z.-Y. Benzene-Based Polyorganodisulfide Cathode Materials for Secondary Lithium Batteries. *Electrochim. Acta* **2006**, *51* (13), 2589−2593.
(9) Oyama, N.; Tatsuma, T.; Sato, T.; Sotomura, T. Dimercaptan−Polyaniline Composite Electrodes for Lithium Batteries with High Energy Density. *Nature* **1995**, *373* (6515), 598−600.
(10) Lu, Y.; Chen, J. Prospects of Organic Electrode Materials for Practical Lithium Batteries. *Nat. Rev. Chem. 2020 43* **2020**, *4* (3), 127−142.
(11) Schon, T. B.; McAllister, B. T.; Li, P. F.; Seferos, D. S. The Rise of Organic Electrode Materials for Energy Storage. *Chem. Soc. Rev.* **2016**, *45* (22), 6345−6404.
(12) Lu, Y.; Zhang, Q.; Li, L.; Niu, Z.; Chen, J. Design Strategies toward Enhancing the Performance of Organic Electrode Materials in Metal-Ion Batteries. *Chem.* **2018**, *4* (12), 2786−2813.
(13) Song, Z.; Zhou, H. Towards Sustainable and Versatile Energy Storage Devices: An Overview of Organic Electrode Materials. *Energy Environ. Sci.* **2013**, *6* (8), 2280−2301.
(14) Liang, Y.; Yao, Y. Positioning Organic Electrode Materials in the Battery Landscape. *Joule* **2018**, *2* (9), 1690−1706.
(15) Wang, C. Weak Intermolecular Interactions for Strengthening Organic Batteries. *Energy Environ. Mater.* **2020**, *3* (4), 441−452.
(16) Xie, J.; Zhang, Q. Recent Progress in Multivalent Metal (Mg, Zn, Ca, and Al) and Metal-Ion Rechargeable Batteries with Organic Materials as Promising Electrodes. *Small* **2019**, *15* (15), 1−20.
(17) Shadike, Z.; Tan, S.; Wang, Q. C.; Lin, R.; Hu, E.; Qu, D.; Yang, X. Q. Review on Organosulfur Materials for Rechargeable Lithium Batteries. *Mater. Horizons* **2021**, *8* (2), 471−500.
(18) Antonello, S.; Daasbjerg, K.; Jensen, H.; Taddei, F.; Maran, F. Formation and Cleavage of Aromatic Disulfide Radical Anions. *J. Am. Chem. Soc.* **2003**, *125* (48), 14905−14916.
(19) Liu, M.; Visco, S. J.; De Jonghe, L. C. Electrochemical Properties of Organic Disulfide/Thiolate Redox Couples. *J. Electrochem. Soc.* **1989**, *136* (9), 2570−2575.
(20) Visco, S. J.; DeJonghe, L. C. Ionic Conductivity of Organosulfur Melts for Advanced Storage Electrodes. *J. Electrochem. Soc.* **1988**, *135* (12), 2905−2909.
(21) Shouji, E.; Yokoyama, Y.; Pope, J. M.; Oyama, N.; Buttry, D. A. Electrochemical and Spectroscopic Investigation of the Influence of Acid−Base Chemistry on the Redox Properties of 2,5-Dimercapto-1,3,4-Thiadiazole. *J. Phys. Chem. B* **1997**, *101* (15), 2861−2866.
(22) Tatsuma, T.; Yokoyama, Y.; Buttry, D. A.; Oyama, N. Electrochemical Polymerization and Depolymerization of 2,5-Dimercapto-1,3,4-Thiadiazole. QCM and Spectroscopic Analysis. *J. Phys. Chem. B* **1997**, *101* (38), 7556−7562.
(23) Kiya, Y.; Hutchison, G. R.; Henderson, J. C.; Sarukawa, T.; Hatozaki, O.; Oyama, N.; Abruña, H. D. Elucidation of the Redox Behavior of 2,5-Dimercapto-1,3,4-Thiadiazole (DMcT) at Poly(3,4-Ethylenedioxythiophene) (PEDOT)-Modified Electrodes and Application of the DMcT - PEDOT Composite Cathodes to Lithium/Lithium Ion Batteries. *Langmuir* **2006**, *22* (25), 10554−10563.
(24) Pope, J. M.; Oyama, N. Organosulfur/Conducting Polymer Composite Cathodes: I. Voltammetric Study of the Polymerization and Depolymerization of 2,5-Dimercapto-1,3,4-thiadiazole in Acetonitrile. *J. Electrochem. Soc.* **1998**, *145* (6), 1893−1901.
(25) Oyama, N.; Kiya, Y.; Hatozaki, O.; Morioka, S.; Abruña, H. D. Dramatic Acceleration of Organosulfur Redox Behavior by Poly(3,4-Ethylenedioxythiophene). *Electrochem. Solid-State Lett.* **2003**, *6* (12), A286.
(26) Kiya, Y.; Henderson, J. C.; Hutchison, G. R.; Abruña, H. D. Synthesis, Computational and Electrochemical Characterization of a Family of Functionalized Dimercaptothiophenes for Potential Use as High-Energy Cathode Materials for Lithium/Lithium-Ion Batteries. *J. Mater. Chem.* **2007**, *17* (41), 4366−4376.
(27) Wang, D. Y.; Guo, W.; Fu, Y. Organosulfides: An Emerging Class of Cathode Materials for Rechargeable Lithium Batteries. *Acc. Chem. Res.* **2019**, *52* (8), 2290−2300.
(28) Liu, M.; Visco, S. J.; De Jonghe, L. C. Novel Solid Redox Polymerization Electrodes: All-Solid-State, Thin-Film, Rechargeable Lithium Batteries. *Journal of The Electrochemical. Society.* **1991**, *138*, 1891−1895.

(29) Liu, M.; Visco, S. J.; De Jonghe, L. C. Novel Solid Redox Polymerization Electrodes: Electrochemical Properties. *J. Electrochem. Soc.* **1991**, *138* (7), 1896−1901.
(30) Kiya, Y.; Hutchison, G. R.; Henderson, J. C.; Sarukawa, T.; Hatozaki, O.; Oyama, N.; Abruña, H. D. Elucidation of the Redox Behavior of 2,5-Dimercapto-1,3,4-Thiadiazole (DMcT) at Poly(3,4-Ethylenedioxythiophene) (PEDOT)-Modified Electrodes and Application of the DMcT - PEDOT Composite Cathodes to Lithium/Lithium Ion Batteries. *Langmuir* **2006**, *22* (25), 10554−10563.
(31) Rodríguez-Calero, G. G.; Lowe, M. A.; Kiya, Y.; Abruña, H. D. Electrochemical and Computational Studies on the Electrocatalytic Effect of Conducting Polymers toward the Redox Reactions of Thiadiazole-Based Thiolate Compounds. *J. Phys. Chem. C* **2010**, *114* (13), 6169−6176.
(32) Yang, L.; Huang, X.; Gogoll, A.; Strømme, M.; Sjödin, M. Conducting Redox Polymer Based Anode Materials for High Power Electrical Energy Storage. *Electrochim. Acta* **2016**, *204*, 270−275.
(33) Vlad, A.; Arnould, K.; Ernould, B.; Sieuw, L.; Rolland, J.; Gohy, J. F. Exploring the Potential of Polymer Battery Cathodes with Electrically Conductive Molecular Backbone. *J. Mater. Chem. A* **2015**, *3* (21), 11189−11193.
(34) Sterby, M.; Emanuelsson, R.; Huang, X.; Gogoll, A.; Strømme, M.; Sjödin, M. Characterization of PEDOT-Quinone Conducting Redox Polymers for Water Based Secondary Batteries. *Electrochim. Acta* **2017**, *235*, 356−364.
(35) Casado, N.; Hernández, G.; Veloso, A.; Devaraj, S.; Mecerreyes, D.; Armand, M. PEDOT Radical Polymer with Synergetic Redox and Electrical Properties. *ACS Macro Lett.* **2016**, *5* (1), 59−64.
(36) Rodríguez-Calero, G. G.; Conte, S.; Lowe, M. A.; Gao, J.; Kiya, Y.; Henderson, J. C.; Abruña, H. D. Synthesis and Characterization of Poly-3,4-Ethylenedioxythiophene/2,5-Dimercapto-1,3,4-Thiadiazole (PEDOT-DMcT) Hybrids. *Electrochim. Acta* **2015**, *167*, 55−60.
(37) Mumtaz, M.; De Cuendias, A.; Putaux, J. L.; Cloutet, E.; Cramail, H. Synthesis of PEDOT Nanoparticles and Vesicles by Dispersion Polymerization in Alcoholic Media. *Macromol. Rapid Commun.* **2006**, *27* (17), 1446−1453.
(38) Lei, Y.; Oohata, H.; Kuroda, S. I.; Sasaki, S.; Yamamoto, T. Highly Electrically Conductive Poly(3,4-Ethylenedioxythiophene) Prepared via High-Concentration Emulsion Polymerization. *Synth. Met.* **2005**, *149* (2−3), 211−217.
(39) Dai, C.; Chang, C.; Chi, H.; Chien, H.; Su, W.; Chiu, W. Emulsion Synthesis of Nanoparticles Containing PEDOT Using Conducting Polymeric Surfactant: Synergy for Colloid Stability and Intercalation Doping. *J. Polym. Sci. Part A. Polym. Chem.* **2008**, *46* (7), 2536−2548.
(40) He, J.; Su, J.; Wang, J.; Zhang, L. Synthesis of Water-Free PEDOT with Polyvinylpyrrolidone Stabilizer in Organic Dispersant System. *Org. Electron.* **2018**, *53*, 117−126. (October 2017)
(41) Li, C.; Huang, S.; Min, C.; Du, P.; Xia, Y.; Yang, C.; Huang, Q. Highly Productive Synthesis, Characterization, and Fluorescence and Heavy Metal Ion Adsorption Properties of Poly(2,5-Dimercapto-1,3,4- Thiadiazole) Nanosheets. *Polymers (Basel).* **2018**, *10* (1), 24.
(42) Zozoulenko, I.; Singh, A.; Singh, S. K.; Gueskine, V.; Crispin, X.; Berggren, M. Polarons, Bipolarons, and Absorption Spectroscopy of PEDOT. *ACS Appl. Polym. Mater.* **2019**, *1* (1), 83−94.
(43) Grocke, G. L.; Zhang, H.; Kopfinger, S. S.; Patel, S. N.; Rowan, S. J. Synthesis and Characterization of Redox-Responsive Disulfide Cross-Linked Polymer Particles for Energy Storage Applications. *ACS Macro Lett.* **2021**, *10* (12), 1637.
(44) Gao, J.; Lowe, M. A.; Conte, S.; Burkhardt, S. E.; Abruña, H. D. Poly(2,5-Dimercapto-1,3,4-Thiadiazole) as a Cathode for Rechargeable Lithium Batteries with Dramatically Improved Performance. *Chem. - A Eur. J.* **2012**, *18* (27), 8521−8526.
(45) Rebetez, G.; Bardagot, O.; Affolter, J.; Réhault, J.; Banerji, N. What Drives the Kinetics and Doping Level in the Electrochemical Reactions of PEDOT:PSS? *Adv. Funct. Mater.* **2022**, *32* (5), 2105821.
(46) Voss, M. G.; Scholes, D. T.; Challa, J. R.; Schwartz, B. J. Ultrafast Transient Absorption Spectroscopy of Doped P3HT Films: Distinguishing Free and Trapped Polarons. *Faraday Discuss.* **2019**, *216*, 339−362.
(47) Heinze, J.; Frontana-Uribe, B. A.; Ludwigs, S. Electrochemistry of Conducting Polymers-Persistent Models and New Concepts. *Chem. Rev.* **2010**, *110* (8), 4724−4771.
(48) Lin, Y. J.; Ni, W. S.; Lee, J. Y. Effect of Incorporation of Ethylene Glycol into PEDOT:PSS on Electron Phonon Coupling and Conductivity. *J. Appl. Phys.* **2015**, *117* (21), 1−5.
(49) Wang, Y.; Zhou, J.; Yang, R. Thermoelectric Properties of Molecular Nanowires. *J. Phys. Chem. C* **2011**, *115* (49), 24418−24428.
(50) Maeng, J.; Jo, M.; Kang, S. J.; Kwon, M. K.; Jo, G.; Kim, T. W.; Seo, J.; Hwang, H.; Kim, D. Y.; Park, S. J.; et al. Transient Reverse Current Phenomenon in a P-n Heterojunction Comprised of Poly(3,4-Ethylene-Dioxythiophene):Poly(Styrene-Sulfonate) and ZnO Nanowall. *Appl. Phys. Lett.* **2008**, *93* (12), 4−7.
(51) Aurbach, D.; Zaban, A. Impedance Spectroscope of Lithium Electrodes. Part 2. The Behaviour in Propylene Carbonate Solutions - the Significance of the Data Obtained. *J. Electroanal. Chem.* **1994**, *367* (1−2), 15−25.
(52) Macdonald, J. R. Impedance Spectroscopy and Its Use in Analyzing the Steady-State AC Response of Solid and Liquid Electrolytes. *J. Electroanal. Chem. Interfacial Electrochem.* **1987**, *223* (1), 25−50.
(53) Zotti, G.; Zecchin, S.; Schiavon, G.; Vercelli, B.; Berlin, A.; Dalcanale, E.; Groenendaal, L. Potential-Driven Conductivity of Polypyrroles, Poly-N-Alkylpyrroles, and Polythiophenes: Role of the Pyrrole NH Moiety in the Doping-Charge Dependence of Conductivity. *Chem. Mater.* **2003**, *15* (24), 4642−4650.
(54) Pomerantz, Z.; Zaban, A.; Ghosh, S.; Lellouche, J. P.; Garcia-Belmonte, G.; Bisquert, J. Capacitance, Spectroelectrochemistry and Conductivity of Polarons and Bipolarons in a Polydicarbazole Based Conducting Polymer. *J. Electroanal. Chem.* **2008**, *614* (1−2), 49−60.
(55) Street, A.; Salleo, A.; Chabinyc, L. Bipolaron Mechanism for Bias-Stress Effects in Polymer Transistors. *Phys. Rev. B - Condens. Matter Mater. Phys.* **2003**, *68* (8), 1−7.
(56) Hauffman, G.; Vlad, A.; Janoschka, T.; Schubert, U. S.; Gohy, J. F. Nanostructured Organic Radical Cathodes from Self-Assembled Nitroxide-Containing Block Copolymer Thin Films. *J. Mater. Chem. A* **2015**, *3* (38), 19575−19581.
(57) Rohland, P.; Schröter, E.; Nolte, O.; Newkome, G. R.; Hager, M. D.; Schubert, U. S. Redox-Active Polymers: The Magic Key towards Energy Storage−a Polymer Design Guideline Progress in Polymer Science. *Prog. Polym. Sci.* **2022**, *125*, No. 101474.
(58) Li, F.; Gore, D. N.; Wang, S.; Lutkenhaus, J. L. Unusual Internal Electron Transfer in Conjugated Radical Polymers. *Angew. Chem.* **2017**, *129* (33), 9988−9991.
(59) Li, F.; Wang, S.; Zhang, Y.; Lutkenhaus, J. L. Electrochemical Energy Storage in Poly(Dithieno[3,2-b:2′,3′-d]Pyrrole) Bearing Pendant Nitroxide Radicals. *Chem. Mater.* **2018**, *30* (15), 5169−5174.
(60) Olsson, H.; Jämstorp Berg, E.; Strømme, M.; Sjödin, M. Self-Discharge in Positively Charged Polypyrrole−Cellulose Composite Electrodes. *Electrochem. commun.* **2015**, *50*, 43−46.
(61) Mirmohseni, A.; Solhjo, R. Preparation and Characterization of Aqueous Polyaniline Battery Using a Modified Polyaniline Electrode. *Eur. Polym. J.* **2003**, *39* (2), 219−223.
(62) Rehan, H. H. A New Polymer/Polymer Rechargeable Battery: Polyaniline/LiClO4(MeCN)/Poly-1-Naphthol. *J. Power Sources* **2003**, *113* (1), 57−61.
(63) Gueye, M. N.; Carella, A.; Faure-Vincent, J.; Demadrille, R.; Simonato, J.-P. Progress in Understanding Structure and Transport Properties of PEDOT-Based Materials: A Critical Review. *Prog. Mater. Sci.* **2020**, *108*, No. 100616.
(64) Yan, Y.; Ben, L.; Zhan, Y.; Liu, Y.; Jin, Y.; Wang, S.; Huang, X. A Designed Core-Shell Structural Composite of Lithium Terephthalate Coating on Li4Ti5O12 as Anode for Lithium Ion Batteries. *Prog. Nat. Sci. Mater. Int.* **2016**, *26* (4), 368−374.

https://doi.org/10.1021/acs.chemmater.4c02387
Chem. Mater. 2024, 36, 9959−9969

(65) Geaney, H.; O'Dwyer, C. Tailoring Asymmetric Discharge-Charge Rates and Capacity Limits to Extend Li-O2 Battery Cycle Life. *ChemElectroChem.* **2017**, *4* (3), 628−635.
(66) Adams, B. D.; Radtke, C.; Black, R.; Trudeau, M. L.; Zaghib, K.; Nazar, L. F. Current Density Dependence of Peroxide Formation in the Li-O2 Battery and Its Effect on Charge. *Energy Environ. Sci.* **2013**, *6* (6), 1772−1778.
(67) Oh, S. H.; Lee, C. W.; Chun, D. H.; Jeon, J. D.; Shim, J.; Shin, K. H.; Yang, J. H. A Metal-Free and All-Organic Redox Flow Battery with Polythiophene as the Electroactive Species. *J. Mater. Chem. A* **2014**, *2* (47), 19994−19998.

https://doi.org/10.1021/acs.chemmater.4c02387
Chem. Mater. 2024, 36, 9959−9969